# TSUNAMI NEAR THE ISRAELI COAST: PRELIMINARY RESULTS OF NUMERICAL MODELING[1]

**Beisel S.A.**
*Institute of Computational Technologies SB RAS, Novosibirsk, Russia*
*Novosibirsk State University, Novosibirsk, Russia*
*E-mail: beisel_s@ngs.ru*

**Chubarov L.B.**
*Institute of Computational Technologies SB RAS, Novosibirsk, Russia*
*Novosibirsk State University, Novosibirsk, Russia*
*E-mail: chubarov@ict.nsc.ru*

**Kit E.**
*Department of Fluid Mechanics and Heat Transfer, Faculty of Engineering,*
*Tel-Aviv University, Tel-Aviv, Israel*
*E-mail: kit@eng.tau.ac.il*

**Levin A.**
*Coastal and Marine Engineering Research Institute, Haifa, Israel*
*E-mail: lanna@tx.technion.ac.il*

**Shokin Yu.I.**
*Institute of Computational Technologies SB RAS, Novosibirsk, Russia*
*Novosibirsk State University, Novosibirsk, Russia*
*E-mail: shokin@ict.nsc.ru*

**Sladkevich M.**
*Coastal and Marine Engineering Research Institute, Haifa, Israel*
*E-mail: michslad@tx.technion.ac.il*

*The study presents a review of historical tsunamis in the Mediterranean region (more than 500 events). Numerical modeling of the tsunami in Aegean Sea (July of 1956) is carried out by means of original algorithms developed in ICT SB RAS, which have been modified and carefully verified on model problems. Based on historical data analysis, locations of the critical for the Israeli coast tsunamigenic earthquake sources are determined. Their intensities and shapes have been designed to generate extreme events, which can pose a potential threat to the coastal zone. These events and their possible effects on the Israeli and Egyptian coasts are modeled.*

## 1. Brief Review of Historical Tsunami Events in the Mediterranean Sea.

The statistical analysis of historical database shows that some information is doubtful due to its variation from one source to another. Anyway analyzing the

[1] The current project is carried out in the framework of Israeli-Russian joint research supported by the Russian Foundation for Basic Research (RFBR, Projects No. 06-05-72014, 07-05-13583, 06-05-64869), Russian Federation; the Program of Fundamental International Research SB RAS (Projects No. 28, 113); the Program of Government Support of Scientific Research conducted by leading scientific schools of the Russian Federation 931.2008.9; Projects INTAS 06-1000013-9236; and the Ministry of Science and Technology (MOST, Project No.05414151), State of Israel.

available data one can conclude that starting from 2000BC there were more than 500 tsunami events. According to different database, the major part of these events was induced by an earthquake (70%-75%). About 5-10% of tsunamis had volcanic origin, ~2-3% were generated by a landslide, less than 1% had meteorological source, and ~15-20% of the tsunami sources remained unknown. Three major tsunamis with wave amplitude more than 30m had been generated in the Mediterranean Sea during XX century. The first occurred in 1908 within the Strait of Messina (near Sicily, Italy) with more than 80,000 people perished, the second was excited in 1956 by several shakes near the Cyclades archipelago in the southern part of the Aegean Sea, and the last one befell in 1979 with epicenter located in the vicinity of city Nice, Italy. The reasons of formation of such catastrophic waves are still unclear because of insufficient information.

The main tsunamigenic source in the Mediterranean is the submerged seismic activity related to the Afro-Syrian Rift, which is similar to that located near the Sumatra coast and associated with one of the apocalyptic tsunami disaster that occurred in Southeastern Asia.

Following the available historical database most Mediterranean tsunami sources lie along the Hellenic arc. For instance, a massive earthquake between Crete and Rhodes dated 08 August 1303 had induced a strong tsunami wave that engulfed not only these islands but reached even the Levant and Egyptian coasts. Other strongest tsunamis in 1481, 1494, 1810, 1856 and 1870 with epicenter near Crete struck Greece and the eastern Mediterranean as well. The strongest tsunamis in the eastern Mediterranean are excited within the seismically active zones located between the Cyprus arc and the Levant fault. Although historical records show that the eastern Mediterranean is less prone to damaging tsunamis than the other eighteen tsunamigenic regions of the Mediterranean Sea, several significant tsunami events have been observed there.

The second tsunamigenic zone in this region stretches along the Cyprus arc and the southern part of Cyprus. Epicenters of earthquakes that provoke into tsunamis usually lie in shallow and moderate waters, e.g. to the west and southwest of Cyprus. There is archeological evidence in favor of the disastrous tsunami dated 21 July 365 AD following an earthquake in Kurion (Cyprus), which possibly destroyed Kurion. Analysis of seabed sediments in Caesarea (Israel) indicates that this city was destroyed as a result of a tsunami excited by strong earthquake in Cyprus arc on December 13, 115 AD. The waves attacked the Levant Coast were documented in Caesarea and Yavne. Similar events were recorded near Cyprus on February 23, 1995, October 09, 1996, and January 13, 1997.

Another tsunamigenic source may be local submerged or coastal landslide. Historical evidence indicates some cases of several meters drawdown in sea level and sea receding for several hours at a distance of 1-2km following by an abrupt sea return with almost no land invading. Relatively prolonged duration of such events reveals their landslide origin.

Analyzing the cross-shore profiles near the Israeli coast one can suggest several zones with landslide potential which are able to cause sea level depression and shoreline retreat of about 0.5-1.5km. For example, a major worldwide landslide (up to $1000km^3$) seems to occur in the late Pliocene. Moreover, there is historical evidence of about 40 moderate and strong landslides during the Pliocene and Holocene periods. In fact, almost the entire strip that stretches along the Israeli coast (the shelf as well as its sill) possesses a potential of landslide. Spatial and temporal distribution of the local

deposits designates that though the frequency of these events rises, their scale diminishes. Frequent occurrence of landslide movements can be related to high seismic activity in the region, steep bank slopes (~5-6°) and high level of gas content in deposits, which increases their porosity. Two protoslumps, which are suspected for high mobility (sliding) in the future, have been revealed on the Israeli shelf.

A tsunami in the eastern Mediterranean occurred on July 09, 1956, was triggered by an earthquake with magnitude M = 7.5 in the Aegean Sea. The waves reached 15m high in the epicentral region and caused boats being driven onto docks, houses flooded and three persons reported drowned. Away from the epicentral area the waves attenuated rapidly, to 2.5m runup on the eastern coast of Crete and small amplitudes recorded on the Egyptian coast.

## 2. Numerical Modeling of Tsunami Waves in the Mediterranean Sea.

The numerical experiments have been conducted on the grid with 1 and 2 arc-minute bathymetry resolution as well as on the refined grid. The main tests have been performed using the 15 sec grid. In the vicinity of the Israeli coast the bathymetry was replaced by more precise data obtained from the local sources.

The required resolution of bathymetry data has been determined in the course of numerical tests carried out within the area of interest that contains the eastern part of the Mediterranean basin stretching from 30.5E to 36.5E and from 31.0N to 37.0N. The grid resolution used ranges from 2min to 15sec. The basic initial free surface perturbation is set to be sinusoidal wave with one-degree length and one-meter amplitude. Other perturbations used differ from the basic one by their length (twice larger or smaller) or by their amplitude (twice larger or smaller). Initial velocities are assumed to be zero.

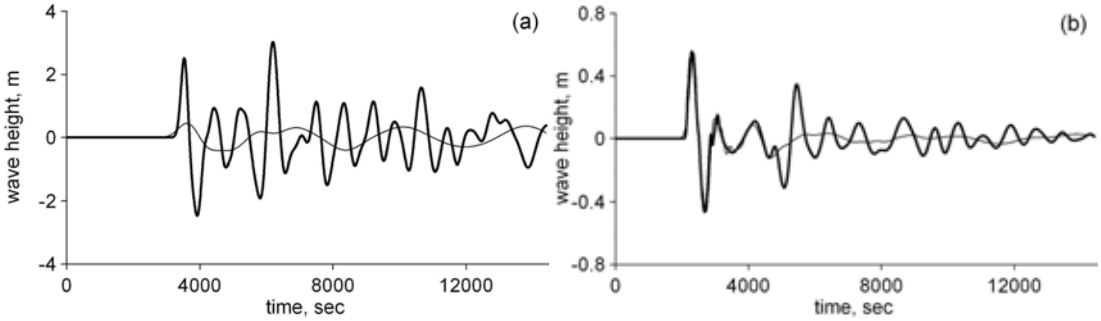


Figure 1. Marigrams for sinusoidal initial perturbation computed at Yafo (a) and offshore Yafo (b). Thin and thick lines correspond to 2min and 15sec grid resolution, respectively.

The obtained results reveal a strong dependence of the characteristics of shallow water marigrams, such as amplitude and frequency, on the length of the original wave or/and may be on the bathymetry resolution. This issue has been investigated in detail. In this respect the dynamics of wave parameters along its path toward the shore has been thoroughly analyzed. As an example, the computed marigrams for the basic perturbation at the monitoring points at Yafo and 10 nodes (1min grid resolution) offshore Yafo are plotted in Fig.1. It appears that close to the shoreline the results are strongly dependent on grid resolution, i.e. the refined grid leads to a few times larger wave amplitude. In deep water there is almost no impact of grid resolution on the leading wave features with the exception of wave tails, which represent the waves reflected from the shore neighboring the source and following the leading wave.

Marigrams in 13 monitoring points along the Israeli coast for all initial perturbations are inherent in this effect. Spectral analysis of this phenomenon (see Fig.2) reveals almost complete lack of high frequencies in the shallow water marigrams, though they present in deep water. At the same time, high frequencies can be preserved utilizing a fine grid. The obtained results show that reliable pictures can be derived only on a fine grid, i.e. at least with 15sec mesh.

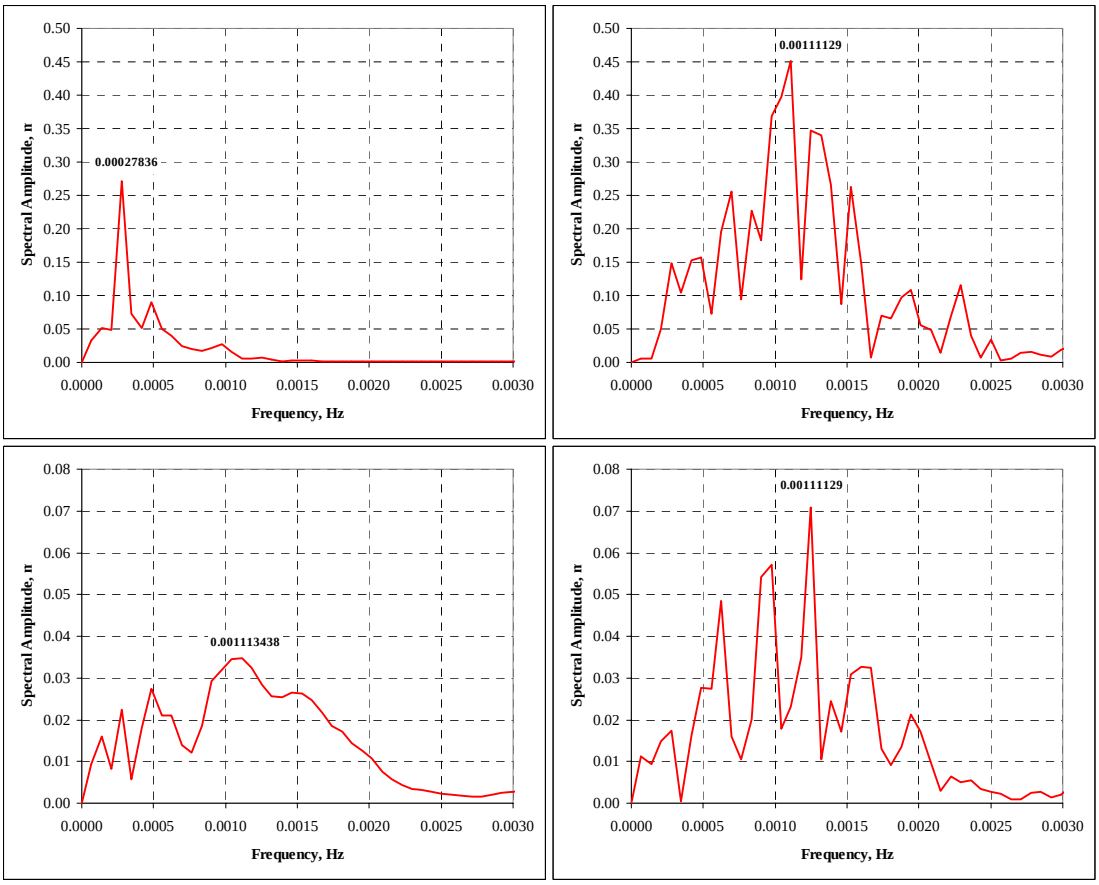


Figure 2. Spectra of marigrams. Top row – marigrams at Yafo; bottom row – deep water marigrams. The left column corresponds to calculations performed on 2min grid and the right column refers to 15sec grid.

# 3. Modeling of the Historical Tsunami of July 09, 1956, Triggered by an Earthquake in the Aegean Sea.

The tsunami occurred on July 09, 1956, was excited by an earthquake in the Aegean Sea, Greece. There were at least 3 major shocks: at 03:12, 03:24 and 06:23 with maximum magnitude 7.5 at 03:24. The waves engulfed mainly the Greece coast, Amorgos Island and Aegean Islands. However, some fluctuations of sea level had been recorded at the Yafo gauge station [1, 2]. The maximum sea level fluctuations associated with the tsunami waves reached ~28cm between 10-11a.m. The sea level oscillations continued ~12 hr with almost the same amplitude. Their visible periods were 12–15 minutes.

Using the well-known relationships and accounting for the geology of the Aegean Sea, the approximated values of the fault length $L$, width $W$ and displacement $D_0$ can be calculated. Analysis of seismic parameters of this tsunamigenic event shows that the length of the fault was about 105km, width ~38km, the azimuth angle ~60° and its vertical displacement ~3m. Using these values and applying the

Gusiakov-Okada model [3, 4] the field of initial displacement of free water surface has been modeled (Fig.3). Initial velocities are assumed to be zero. The specified boundary conditions ensure the free wave propagation through the open boundaries and wave reflection from the coast boundary. Marigrams are computed at 13 points along the Israeli shore.

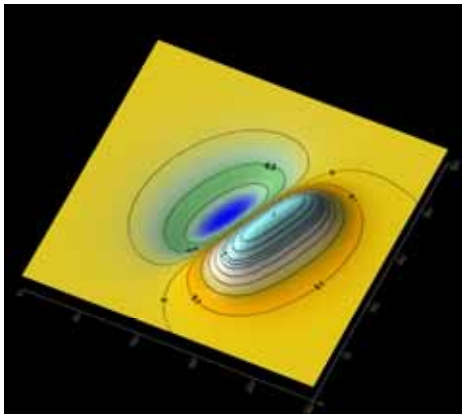

Figure 3. Initial perturbation of free water surface for the 1956 earthquake.

The preliminary simulations are performed within the study basin, which stretches from 24.0E to 36.0E and from 30.5N to 38.0N. The maximum water depth is 4382m (Fig.4).

As shown in the preceding chapter, in order to obtain the reliable results the selected grid should provide the necessary resolution of the numerical algorithm applied. This requirement makes special sense within the littoral zones of the basin. At the same time, implementation of a fine grid within the whole domain results in unreasonable increase in the required computational resources. The marigrams obtained at Yafo through utilizing different computational grids and plotted in Fig.5 show that the features of the leading wave can be preserved even using a coarse grid.

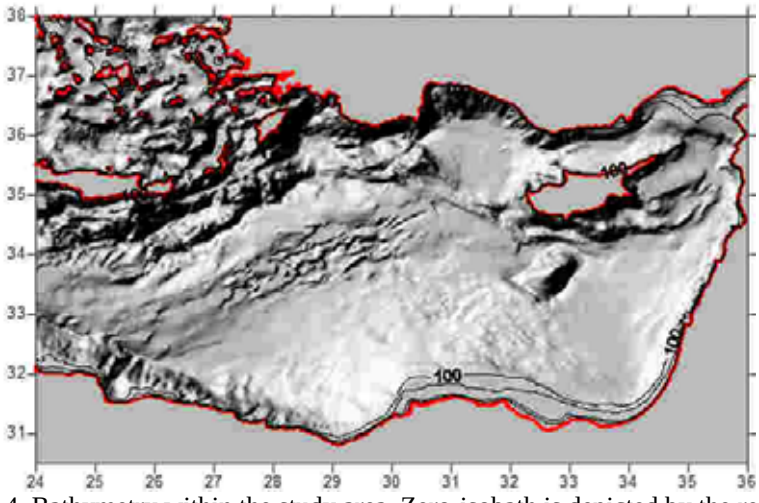


Figure 4. Bathymetry within the study area. Zero-isobath is depicted by the red line.

The efficiency of the recently used common computational techniques can be significantly improved by adaptation of the following methodology. The entire domain $\Omega^h$ is divided into two sub-domains: a deep water sub-domain with coarse grid and a shallow water strip in the proximity to the coastline $\omega^h \subset \Omega^h$, which requires finer grid resolution. $h$ is the space increment of the coarse grid (in our case

$h$ =1min). The computations on the $\Omega^h$ are conducted during the period from 0 to $T_z$. The obtained at time $T_z$ displacement of the free water surface and velocity fields are recalculated to the refined grid and then are used as initial conditions for further computations (from time $T_z$ to $T_{final}$) within $\omega^{h_1}$. $h_1 < h$ is the space increment for fine grid (in our case $h_1 = 15\,\text{sec}$). This methodology based on the results of "freezing" is recommended in cases when the computational domain consists of two sub-domains: a deep basin, where the use of a coarse grid provides reasonable results, and a shallow part, which requires implementation of a finer grid.

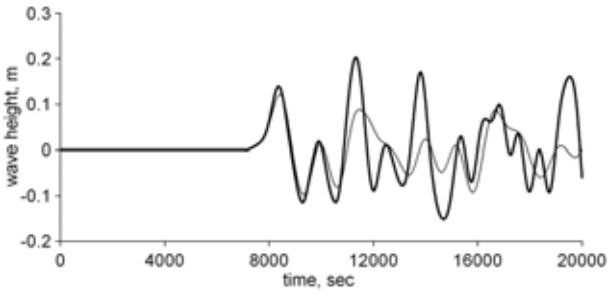


Figure 5. Marigrams for the 1956 tsunami computed at Yafo. Thin and thick lines correspond to 1min and 15sec grid resolution, respectively.

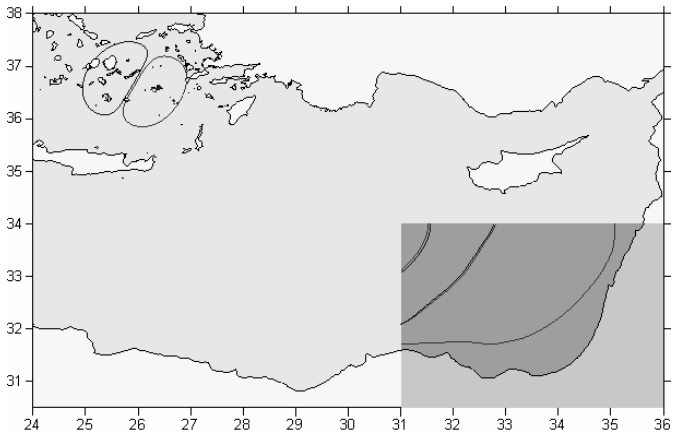


Figure 6. Schematic representation of the computational domain applied in the modeling of the historical tsunami triggered by an earthquake in the Aegean Sea. The position of tsunami generation source is shown by two ellipses, the shadowed area depicts the sub-domain $\omega$, the isolines represent the "frozen" features of the flow field involved in the further more detailed computations.

This methodology has been thoroughly tested for the model and real basins near the Israeli coast as well as in the surroundings of the Kamchatka Peninsula [5]. The results show that the required accuracy can be attained via an adequate choice of the time $T_z$ and the sub-domain $\omega$. This allows one to avoid the accuracy degradation by conducting partial computations on the coarse grid and then neglecting some parts of wave fields while carrying out new computations in smaller sub-domain on a refined grid. Furthermore, this brings about a remarkable reduction in time consumption required for the solution of such complicated problem.

For the discussed computational test, the 1min grid is used until the time $T_z = 5860\,\text{sec}$. During this time the leading wave manages to cross the boundary of the sub-domain $\omega$ limited by 31E, 30.5N and 36E, 34N (Fig.6). After "freezing" and recalculation of the required parameters onto the new refined 15sec grid, the simulations are continued until the time $T_{final}$ =43,200sec is reached.

In order to estimate the data lost as a result of the "freezing" procedure, a comparison of the results obtained using the common 1min grid for the whole domain $\Omega$ with those derived by involving the "freezing" methodology has been carried out. The comparison (Fig.7) shows that, mainly, the features of the leading waves are preserved; however, some decrease in wave amplitude along the marigram tail is observed. This can be a result of wave reflection from the surrounding the source islands. Therefore, the leading wave (extracted using the "freezing" methodology) is followed by smaller waves that are unable to reach the boundary of the sub-domain $\omega$ during the time $T_z$ and, thus, they are lost in the "freezing" routine. Since usually the leading waves have the maximum amplitude and, hence, pose the major treat to the coastal environment and community, the proposed "freezing" methodology is acceptable.

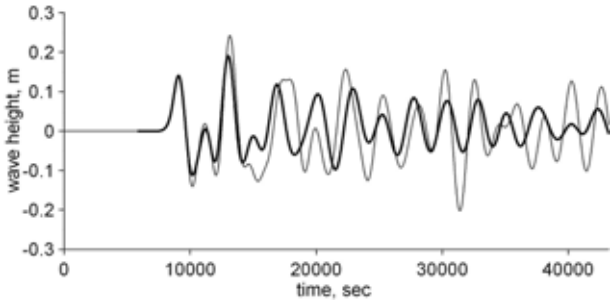


Figure 7. Marigrams obtained on the common 1min grid for the whole domain $\Omega$ (thin line) and using the "freezing" technique (thick line) at the Yafo marigraph.

Analysis of the result obtained on the fine grid shows that the maximum wave amplitudes vary from 10cm to 20cm depending on the monitoring point. For instance, the wave amplitudes near Yafo (Fig.5) are about 25cm, which is in good agreement with tide-gauge records of July 09, 1956.

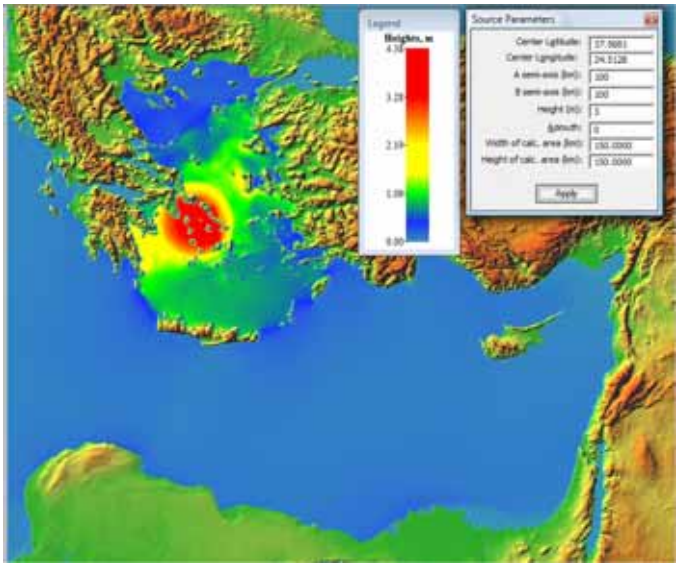

Figure 8. Wave energy propagation for the hypothetical tsunamigenic source generated by an earthquake in the Aegean Sea.

The picture of the tsunami glow from a hypothetical tsunamigenic source (Fig.8) excited by an earthquake in the Aegean Sea, i.e. distribution of maximum wave heights in the course of simulations, indicates that the major part of the wave energy

is trapped by the neighboring archipelagos and, consequently, is almost no felt outside it. Since the Aegean Sea represents one of the main regions of tsunamigenic earthquakes, seismic activity in this basin poses almost no threat to the Israeli coast.

The following investigation is focused on the determination of location of tsunamigenic earthquakes in the basins surrounding Cyprus and the southern part of the Cyprus arc, which are suspected of posing a hazard to the Levant coast.

# 4. Modeling of Hypothetical Tsunamis near the Israeli Coast.

This chapter presents the simulation of hypothetical tsunami events originated from the nearby sources. The considered events correspond to extreme earthquake with magnitude 8. The location of epicenters has been specified through an analysis of the available for this region historical data.

Three of the four considered events are located southward Cyprus and one – close to the Israeli coast. Initial perturbations for all events are simulated using the Gusiakov-Okada model. Five monitoring points along the Egyptian coast, and ten for the first three sources: half – along the trace from the source to the Israeli coast and half – along the trace from the source to the Egyptian coast are added (Fig.9). Some decrease in size of the study domain allows us to conduct simulations on a fine grid without “freezing”.

The main direction of wave energy propagation is well depicted by glow pictures plotted in Fig.10. The maximum wave heights from the first source are obtained in the southern part of the Israeli coast and the eastern part of the Egyptian coast. The energy is partially spread northwestward to the southwest of Cyprus and Turkey. Waves generated by the second source propagate toward Israel, Egypt, southern Cyprus and the eastern Turkish seashore. Waves from the third source are spread in the direction of Israel, Cyprus and the eastern Turkey. Owing to the fourth source location close to Israel, the wave energy concentrates mainly in the Israeli littoral zone and along the Egyptian shore. The similar pictures are obtained for the minimum (maximum negative) wave heights.

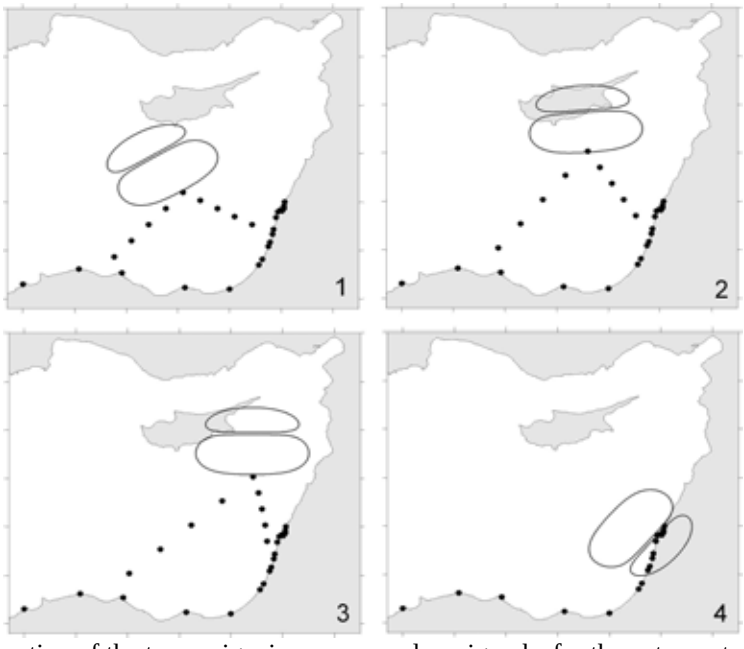


Figure 9. Location of the tsunamigenic sources and marigraphs for the extreme tsunami event modeling.

Comparison between the results obtained for the considered four sources indicates that the greatest hazard to Israel is posed by the last fourth source inherent in nearly 8m wave amplitudes at the northern cities and 7m – at the southern. Maximum drawdown of sea level for this event ranges from 4m to 8m depending on the city location. The second comes the third source with wave amplitudes ~6m near Haifa. The waves initiated by the second source are less than 4m and reach their maximum on the north of the Israeli coast. In contrary, the wave generated by the first source reach their maximum on the south of Israel and are of ~2-3m on the north. Along the Egyptian coast the wave amplitudes diminish gradually along the shore from the east to the west with maximum values range from 4-6m to 1-2m.

Analysis of the results reveals that a fine grid is required mainly for the Egyptian coast and the southern littoral zones of Israel that might be associated with the wide shelf in these regions. The heights of the leading wave there, obtained on the fine grid were three times larger than those computed using the common coarse grid. The difference in the results of two algorithms decreases northward the Israeli coast and westward the Egyptian coast. In respect of spectral characteristics of the obtained marigrams, all of them provide the dominant frequency associated with the source of about 20-30min.

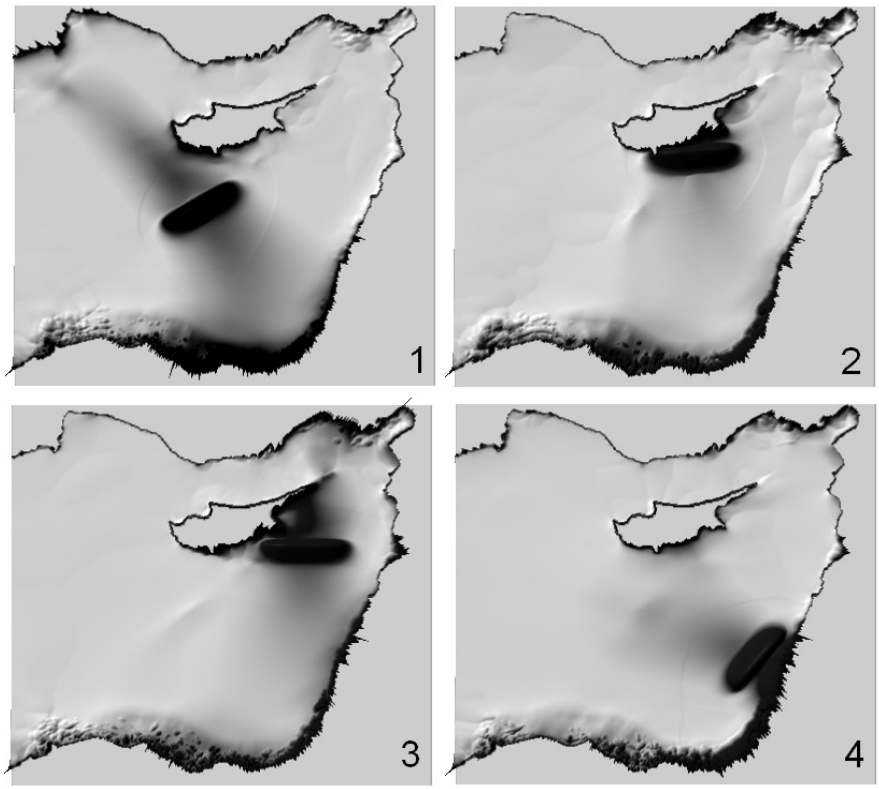


Figure 10. Distribution of the maximum wave heights induced by the four selected extreme sources.

# References

1. Goldsmith V., Gilboa M. Tide in Israel // Ofakim Be'Geograptia, 1986. Vol. 15. P. 21 – 47 (in Hebrew)
2. van Dorn W.G. Tide Gage Response to Tsunamis. Part II: Other Oceans and Smaller Seas // J. of Phys. Oceanography, 1987. Vol. 17. P. 1507-1516.

3. Gusiakov V.K. Interrelation of tsunami waves and source parameters at submarine earthquakes. // In: Mathematical Problems of Geophysics: Proceedings of Computing Center of Siberian Branch of USSR Academy of Sciences. 1974. Issue 5. Part 1. P. 118 – 140.
4. Okada Y. Surface deformation due to shear and tensile faults in the half-space // Bull. Seis. Soc. Am. 1985. V. 75. P. 1135 – 1154.
5. Beisel S.A., Eletsky S.V., Fedotova Z.I., Chubarov L.B. Numerical features of tsunami wave simulation in real water areas // In: Proceedings of the IX All-Russian Conference “Applied technologies of hydroacoustics and hydrophysics”. St. Petersburg: Nauka, 2008, 750 pp. P. 432-436.